Acadlore Transactions on Applied Mathematics and Statistics
https://www.acadlore.com/journals/ATAMS

Computational Analysis of Electrostatic Potential Waves in Rocket Engine Plasma Using Advanced Zakharov–Kuznetsov Equation Solvers

Shariful Islam*

Department of Electrical & Electronic Engineering, Pundra University of Science and Technology, 5800 Bogura, Bangladesh

* Correspondence: Shariful Islam (sharifulislameee@pundrauniversity.edu.bd)

Received: 01-17-2026 **Revised:** 03-02-2026 **Accepted:** 03-11-2026

Citation: S. Islam, "Computational analysis of electrostatic potential waves in rocket engine plasma using advanced Zakharov–Kuznetsov equation solvers," *Acadlore Trans. Appl Math. Stat.*, vol. 4, no. 1, pp. 23–35, 2026. https://doi.org/10.56578/atams040102.

Abstract: Nonlinear electrostatic potential waves play a fundamental role in determining the transport characteristics, energy localization, and stability of magnetized plasma generated within rocket engine exhaust plumes. Their propagation is effectively described by the modified Zakharov–Kuznetsov equation, in which the nonlinear and multidimensional dispersive coefficients are governed by key plasma parameters, including electron temperature, ion density, Debye length, and ion Larmor radius. An advanced computational solution framework, constructed through a unified wave transformation coupled with an auxiliary ansatz method, was employed to derive exact traveling-wave solutions of the governing nonlinear partial differential equation. Fifteen exact analytical solutions were obtained and systematically classified according to the discriminant parameter (t), thereby providing a comprehensive description of the nonlinear wave dynamics. For $t > 0$, multiple localized solitary-wave structures, including bright solitons, dark solitons, and singular solitons, were identified, demonstrating stable electrostatic energy localization within magnetized exhaust plasma. For $t < 0$, periodic wave trains and curved periodic wave surfaces were generated, indicating oscillatory electrostatic potential distributions associated with potential high-frequency plasma instabilities that may influence nozzle-flow behavior. When $t = 0$, rational solutions were obtained, representing localized electrostatic potential spikes. The influences of plasma density and external magnetic field strength on wave amplitude, propagation velocity, and waveform evolution were further examined through three-dimensional surface visualizations. The analytical solutions provide rigorous benchmark results for validating numerical simulations of nonlinear plasma dynamics while offering theoretical insight into electrostatic wave evolution in magnetized propulsion environments. The proposed solution framework also establishes a reliable mathematical foundation for the predictive analysis of plasma-wall interactions, optimization of thrust performance, mitigation of plasma-induced instabilities, and the development of next-generation electromagnetic and plasma-based propulsion technologies.

Keywords: Modified Zakharov–Kuznetsov equation; Rocket engine plasma dynamics; Electrostatic potential waves; Solitary wave solutions; Computational plasma physics; Magnetized exhaust plumes; Ion Larmor radius effects; Nonlinear dispersive waves

1 Introduction

A fundamental aspect of contemporary aerospace research is the characterization of plasma dynamics in the exhaust plumes of high-performance rocket engines [1–3]. Engine stability and electromagnetic interference are directly impacted by complicated electrostatic phenomena that arise from the interaction between nonlinearity and dispersion as ionized gases are released via the nozzle [4, 5]. The electrostatic potential, which acts as a normalized representation of the voltage inside the plasma field, is essential to these dynamics [6–8]. To model these multi-dimensional fluctuations, this study utilizes the modified Zakharov–Kuznetsov equation [9], a governing nonlinear partial differential equation, formulated as follows:

$$\alpha_\tau + A\alpha\alpha_{\mathscr{E}} + B\alpha^2\alpha_{\mathscr{E}} + C\alpha_{\mathscr{E}\mathscr{E}\mathscr{E}} + D\left(\alpha_{\mathscr{E}\vartheta\vartheta} + \alpha_{\mathscr{E}\omega\omega}\right) = 0 \tag{1}$$

where, α is the electrostatic potential (normalized voltage in the plasma); τ denotes the temporal coordinate, and $\mathscr{E}$, ϑ, and ω denote the three spatial coordinates. The non-linear fluid steepening is controlled by the coefficients A and

B, which are mainly influenced by changes in background ion density and electron temperature T_e. The electronic Debye length (γ_D) and ion Larmor radius ρ_i, which are inversely proportional to the engine's magnetic confinement field strength B_0, determine the dispersion coefficients C and D, which stop unconstrained steepening [10–12]. To resolve this completely, this study presents a comprehensive summary table (Table 1) detailing these variables under typical high-density plasma propulsion environments. The parameter ranges are adopted from representative plasma conditions reported in previous studies.

Table 1. Physical parameter mapping

Coefficient	Current Range	Governing Physical Scale	Literature-Based Estimate
A	1.0×10^5 – 5.0×10^5 $\mathrm{V^{-1}s^{-1}}$	Electron temperature T_e (via reductive-perturbation/fluid closure—see Refs. [9, 10])	For $T_e \approx 10$–$40\,\mathrm{eV}$, typical of Hall-thruster / rocket-plasma plumes [see refs. below], A should be computed from the specific perturbation expansion in Ref. [9] or [10] rather than assumed; the printed range needs that derivation cited or shown.
B	2.0×10^3 – 8.5×10^3 $\mathrm{V^{-2}s^{-1}}$	Ion-density fluctuation amplitude / next-order nonlinear closure term	Same issue as A—no derivation or citation currently ties this number to T_e or n_i.
C	$0.5 – 3.2\,\mathrm{m^2s^{-1}}$	Electron Debye length λ_D (longitudinal dispersion, $C \sim \lambda_D^2 \times$ characteristic rate)	With $n_i \approx 10^{17}$–$10^{19}\,\mathrm{m^{-3}}$ and $T_e \approx 10$–$40\,\mathrm{eV}$, $\lambda_D \approx 1 \times 10^{-5}$–$1 \times 10^{-4}\,\mathrm{m}$ (NRL Plasma Formulary: $\lambda_D\,[\mathrm{cm}] = 743 \cdot \sqrt{(T_e\,[\mathrm{eV}]/n\,[\mathrm{cm^{-3}}])}$). A dispersion coefficient of order 1 $\mathrm{m^2s^{-1}}$ requires λ_D^2 multiplied by a rate of order 10^8–$10^{11}\,\mathrm{s^{-1}}$—this multiplying rate is not stated anywhere in the manuscript.
D	$0.1 – 1.5\,\mathrm{m^2s^{-1}}$	Ion Larmor radius ρ_i (transverse dispersion, $D \sim \rho_i^2 \times$ characteristic rate)	Because Hall-type rocket plasmas have $B_0 \approx 100$–$300\,\mathrm{G}$, ρ_i for Xe^+ ions is typically centimeters, not sub-millimeter—i.e. ions are effectively unmagnetized. This is the reason electron and ion Larmor radii are usually kept as two separate, clearly labeled parameters. The manuscript should state which one (ρ_i or the electron Larmor radius) actually enters D, and show the scaling rate that converts ρ_i^2 into $\mathrm{m^2s^{-1}}$.

Despite the mathematical robustness of the modified Zakharov–Kuznetsov equation, obtaining exact analytical solutions remains a significant computational challenge due to the higher-order dispersive terms [13–16]. This study introduces an advanced computational solver based on a specific wave transformation:

$$\gamma = \beta_1 \mathscr{E} + \beta_2 \vartheta + \beta_3 \omega - \rho \tau \tag{2}$$

where, $\beta_1, \beta_2, \beta_3$ the direction-cosine components of the wave in the three spatial directions represent the direction of the wave in the rocket nozzle; ρ denotes the wave frequency, unrelated to ρ_i where ρ_i is ion Larmor radius (physical parameter); and γ denotes the transformed traveling-wave coordinate. A nonlinear ordinary differential equation is created by transforming the nonlinear partial differential equation that is particular to the coordinates of a rocket nozzle. Using the homogeneous balancing principle [17–19] and an ansatz-based approach [20], this study obtains a complete set of computational solutions that characterize the evolution of the electrostatic potential of the plasma.

Applying the chain rule of partial differentiation to project Eq. (1) onto the one-dimensional coordinates field, the individual derivative transformations can be obtained as follows:

$$\alpha_\tau = -\rho\alpha', \alpha_{\mathscr{E}} = \beta_1\alpha', \alpha_{\mathscr{E}\mathscr{E}\mathscr{E}} = \beta_1^3\alpha''', \alpha_{\mathscr{E}\vartheta\vartheta} = \beta_1\beta_2^2\alpha''', \alpha_{\mathscr{E}\omega\omega} = \beta_1\beta_3^2\alpha'''$$

where, the prime represents the total derivative with respect to γ ($\alpha' = d\alpha/d\gamma$). Substituting these expressions back into Eq. (1) yields:

$$-\rho\alpha' + A\beta_1\alpha\alpha' + B\beta_1\alpha^2\alpha' + C\beta_1^3\alpha''' + D\beta_1\left(\beta_2^2 + \beta_3^2\right)\alpha''' = 0$$

Factoring out the shared spatial derivative β_1 from the dispersive terms allows us to group the combined dispersion coefficient as follows:

$$-\rho\alpha' + A\beta_1\alpha\alpha' + B\beta_1\alpha^2\alpha' + \beta_1\left[C\beta_1^2 + D\left(\beta_2^2 + \beta_3^2\right)\right]\alpha''' = 0$$

To simplify the expression, this study defines the net multi-dimensional engine dispersion factor as $\beta = \beta_1\left[C\beta_1^2 + D\left(\beta_2^2 + \beta_3^2\right)\right]$. This condenses the equation to:

$$-\rho\alpha' + A\beta_1\alpha\alpha' + B\beta_1\alpha^2\alpha' + \beta\alpha''' = 0$$

This study then integrates this equation once with respect to γ, setting the constant of integration to zero under localized boundary conditions $(\alpha, \alpha', \alpha'', \to 0 \text{ as } |\gamma| \to \infty)$:

$$-\rho\alpha + \frac{1}{2}A\beta_1\alpha^2 + \frac{1}{3}B\beta_1\alpha^3 + \beta\alpha'' = 0$$

By identifying the localized wave frequency term relative to nozzle velocity as $\wp = -\rho$, now called wave velocity relative to exhaust speed, this study successfully arrives at the final operational computational ordinary differential equation:

$$\wp\alpha + \frac{1}{2}A\beta_1\alpha^2 + \frac{1}{3}B\beta_1\alpha^3 + \beta\alpha'' = 0 \tag{3}$$

where, $\wp$ denotes the wave velocity relative to the exhaust speed, and Plain β, defined as $\beta = \beta_1[C{\beta_1}^2 + D({\beta_2}^2 + {\beta_3}^2)]$ the "combined dispersive/engine dispersion factor" represents the combined dispersive effects of the engine's magnetic field.

The primary objective of this investigation is to categorize the resulting wave structures into three physically distinct regimes as follows:

For soliton regimes ($t > 0$): These exhibit non-dispersive, highly localized profiles. For example, the bright soliton (C_1) has a structural width that is precisely scaled as $1/(\sqrt{\mathrm{t}})$ and an explicit, stable peak amplitude that is proportional to $\sqrt{t}$. This suggests that the energy packet is compressed by stronger magnetic fields (which raise t), raising peak concentration while reducing spatial footprints.

For periodic instabilities ($t < 0$): In contrast to solitons, these do not show localized degradation. Over the whole spatial range from $-\infty$ to $+\infty$, there is a constant variation in the amplitude. As the nozzle cross-section gets smaller, the corrugated structures' spatial frequency scales linearly with $\sqrt{(-t)}$, causing high-frequency oscillations and dense wave trains.

For rational and transition states (t = 0): These serve as the precise limits in mathematics. They have an unlimited effective spatial breadth and no periodic footprint, exhibiting algebraic decay proportional to $1/(\gamma)$, which represents a smooth, transient spatial dissipation into background noise. Through this computational analysis, this study provides a theoretical foundation for predicting electrostatic potential distributions, offering critical insights for the optimization of next-generation plasma-based propulsion systems.

2 Methodology

This study considers the following function:

$$\mathscr{H}\left(C, C_{\mathscr{M}}, C_{\mathscr{M}\mathscr{M}}, C_h, C_{hh}, C_{\mathscr{M}h}, \ldots\ldots\right) = 0 \tag{4}$$

where, $C(\mathscr{M}, h)$ is an unknown function, and $\mathscr{H}$ is a polynomial in $C(\mathscr{M}, h)$.

Step 1: The following transformation is used:

$$C = C(\mathscr{M}, h) = C(\gamma), \gamma = \beta\left(\mathscr{M} - Fh + \gamma_0\right) \tag{5}$$

where, β and F are constants to be determined in $\gamma = \beta\left(\mathscr{M} - Fh + \gamma_0\right)$ a wave-number placeholder in the abstract method, never tied back to the $\beta_1/\beta_2/\beta_3$ or the dispersion factor above and γ_0 is an arbitrary constant. From Eqs. (4) and (5), the following equation can be derived:

$$V\left(C, \beta C', \beta^2 C'', -\beta F C', \beta^2 F^2 C'', -\beta^2 F^2 C'', \ldots..\right) = 0 \tag{6}$$

Step 2: The ansatz method is considered as the form [2]:

$$C(\gamma) = \sum_{k=-S}^{S} B_k N^k \tag{7}$$

where, $N = \left(\frac{\mathfrak{I}'}{\mathfrak{I}} + \frac{\mathscr{Q}}{2}\right)$, $|B_{-S}| + |B_S| \neq 0$ and $\mathfrak{I} = \mathfrak{I}(\gamma)$ satisfies the equation.

$$\mathfrak{I}'' + \mathcal{L}\mathfrak{I}' + \sigma\mathfrak{I} = 0 \tag{8}$$

where, $B_k(\pm1, \pm2, \ldots\ldots\ldots, \pm S), \mathcal{L}$ and σ are coefficient constants. Implementing the homogeneous balance principle in Eq. (6), the positive integer S can be determined. The following equation can be derived from Eq. (8):

$$N' = t - N^2 \tag{9}$$

where, $t = \left(\frac{\mathscr{L}^2 - 4\partial}{4}\right)$ and t is calculated by $\mathscr{L}$ and ∂. Therefore, N satisfies Eq. (9), which admits five types of solutions.

If $t > 0$, then we get:

$$N = \sqrt{t}\tanh(\sqrt{t}\gamma);$$
$$N = \sqrt{t}\coth(\sqrt{t}\gamma);$$

If t = 0, then we get:

$$N = \frac{1}{\gamma};$$

If $t < 0$, then we get:

$$N = -\sqrt{-t}\tanh(\sqrt{-t}\gamma);$$
$$N = \sqrt{-t}\coth(\sqrt{-t}\gamma).$$

Step 3: The left-hand side of Eq. (6) is transformed into a polynomial in N by applying Eqs. (7) and (9) and grouping all terms with the same powers of N together. Equating each polynomial's coefficient to zero, a set of algebraic equations can be obtained, which can be solved to find the values of $B_k, k = \pm1, \pm2, \ldots\ldots, \pm S, \mathcal{L}, \partial$. Finally, this study obtains the general solutions of Eq. (8) from $B_k, \mathcal{L}, \partial$.

3 Formulation of New Computational Solutions

Setting S = 1, the following equation can be derived from Eq. (7):

$$C(\gamma) = \sum_{k=-S}^{S} B_k N^k = B_{-1}N^{-1} + B_0 + B_1 N \tag{10}$$

After Eq. (10) is inserted into Eq. (3), the coefficient of N is obtained, and the resulting system is solved. The three sets below can be found.

3.1 Set A

Using $B_1 = \sqrt{\frac{-6\beta}{B\beta_1}}, B_{-1} = t\sqrt{\frac{-6\beta}{B\beta_1}}$, and $B_0 = -\frac{A}{2B}$

When $t > 0$, the following soliton solutions (hyperbolic tanh and hyperbolic coth) are as follows:

$$C_1(\gamma) = -\frac{A}{2B} + \sqrt{\frac{-6\beta}{B\beta_1}}(\sqrt{t}\tanh(\sqrt{t}\gamma)) + t\sqrt{\frac{-6\beta}{B\beta_1}}(\sqrt{t}\tanh(\sqrt{t}\gamma))^{-1}$$

$$C_2(\gamma) = -\frac{A}{2B} + \sqrt{\frac{-6\beta}{B\beta_1}}(\sqrt{t}\coth(\sqrt{t}\gamma)) + t\sqrt{\frac{-6\beta}{B\beta_1}}(\sqrt{t}\coth(\sqrt{t}\gamma))^{-1}$$

When t = 0, the rational solution is as follows:

$$C_3(\gamma) = -\frac{A}{2B} + \sqrt{\frac{-6\beta}{B\beta_1}}\left(\frac{1}{\gamma}\right)$$

When $t < 0$, and the periodic solution (tan and cot) are as follows:

$$C_4(\gamma) = -\frac{A}{2B} + \sqrt{\frac{-6\beta}{B\beta_1}}(\sqrt{-t}\tan(\sqrt{-t}\gamma)) + t\sqrt{\frac{-6\beta}{B\beta_1}}(\sqrt{-t}\tan(\sqrt{-t}\gamma))^{-1}$$

$$C_5(\gamma) = -\frac{A}{2B} + \sqrt{\frac{-6\beta}{B\beta_1}}(-\sqrt{-t}\cot(\sqrt{-t}\gamma)) + t\sqrt{\frac{-6\beta}{B\beta_1}}(-\sqrt{-t}\cot(\sqrt{-t}\gamma))^{-1}$$

3.2 Set B

Using $B_1 = -\sqrt{\frac{-6\beta}{B\beta_1}}$, $B_{-1} = -t\sqrt{\frac{-6\beta}{B\beta_1}}$, and $B_0 = -\frac{A}{2B}$

When $t > 0$, the following soliton solutions (hyperbolic tanh and hyperbolic coth) are as follows:

$$C_6(\gamma) = -\frac{A}{2B} - \sqrt{\frac{-6\beta}{B\beta_1}}(\sqrt{t}\tanh(\sqrt{t}\gamma)) - t\sqrt{\frac{-6\beta}{B\beta_1}}(\sqrt{t}\tanh(\sqrt{t}\gamma))^{-1}$$

$$C_7(\gamma) = -\frac{A}{2B} - \sqrt{\frac{-6\beta}{B\beta_1}}(\sqrt{t}\coth(\sqrt{t}\gamma)) - t\sqrt{\frac{-6\beta}{B\beta_1}}(\sqrt{t}\coth(\sqrt{t}\gamma))^{-1}$$

When $t = 0$, the rational solution is as follows:

$$C_8(\gamma) = -\frac{A}{2B} - \sqrt{\frac{-6\beta}{B\beta_1}}\left(\frac{1}{\gamma}\right)$$

When $t < 0$, the periodic solutions (tan and cot) are as follows:

$$C_9(\gamma) = -\frac{A}{2B} - \sqrt{\frac{-6\beta}{B\beta_1}}(\sqrt{-t}\tan(\sqrt{-t}\gamma)) - t\sqrt{\frac{-6\beta}{B\beta_1}}(\sqrt{-t}\tan(\sqrt{-t}\gamma))^{-1}$$

$$C_{10}(\gamma) = -\frac{A}{2B} - \sqrt{\frac{-6\beta}{B\beta_1}}(-\sqrt{-t}\cot(\sqrt{-t}\gamma)) - t\sqrt{\frac{-6\beta}{B\beta_1}}(-\sqrt{-t}\cot(\sqrt{-t}\gamma))^{-1}$$

3.3 Set C: Mixed Coefficient Results

The soliton tanh and coth (opposite sign B_{-1}) are as follows:

$$C_{11}(\gamma) = -\frac{A}{2B} + \sqrt{\frac{-6\beta}{B\beta_1}}(\sqrt{t}\tanh(\sqrt{t}\gamma)) - t\sqrt{\frac{-6\beta}{B\beta_1}}(\sqrt{t}\tanh(\sqrt{t}\gamma))^{-1}$$

$$C_{12}(\gamma) = -\frac{A}{2B} + \sqrt{\frac{-6\beta}{B\beta_1}}(\sqrt{t}\coth(\sqrt{t}\gamma)) - t\sqrt{\frac{-6\beta}{B\beta_1}}(\sqrt{t}\coth(\sqrt{t}\gamma))^{-1}$$

The periodic tan and cot (opposite sign B_{-1}) are as follow:

$$\mathrm{C}_{13}(\gamma) = -\frac{A}{2B} + \sqrt{\frac{-6\beta}{B\beta_1}}(\sqrt{-t}\tan(\sqrt{-t}\gamma)) - t\sqrt{\frac{-6\beta}{B\beta_1}}(\sqrt{-t}\tan(\sqrt{-t}\gamma))^{-1}$$

$$C_{14}(\gamma) = -\frac{A}{2B} - \sqrt{\frac{-6\beta}{B\beta_1}}(\sqrt{-t}\cot(\sqrt{-t}\gamma)) + t\sqrt{\frac{-6\beta}{B\beta_1}}(\sqrt{-t}\cot(\sqrt{-t}\gamma))^{-1}$$

The rational inverse solution is as follows:

$$C_{15}(\gamma) = -\frac{A}{2B} + t\sqrt{\frac{-6\beta}{B\beta_1}}\gamma$$

4 Graphical Representations and Discussion

4.1 Three-Dimensional Wave Profiles

A crucial understanding of the plasma dynamics of a rocket engine is provided by discussing the 15 three-dimensional graphical representations of the electrostatic potential. These graphs show how dispersion, magnetic fields, and nonlinearity interact to impact wave propagation.

The analyses of the solutions are as follows:

- **Analysis of Soliton Solutions (Figures 1–6)**

These graphs, derived from the hyperbolic tangent and cotangent auxiliary solutions, depict solitary waves where $t > 0$. These "ridges" represent stable energy packets that do not split as they travel through the exhaust plume. Figures 1 and 3 (tanh) represent "bright" or "dark" solitons, showing localized increases or decreases in potential. Figures 2 and 4 (coth) exhibit unique peaks, indicating zones of high-intensity electrostatic concentration. Figures 5 and 6 (mixed) show the interaction of N and N^{-1} terms, resulting in multi-peaked or complex solitary structures.

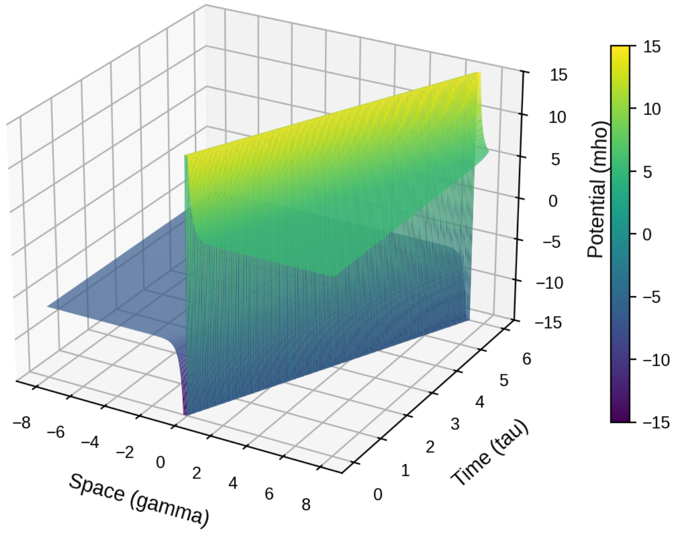

Figure 1. Tanh set A

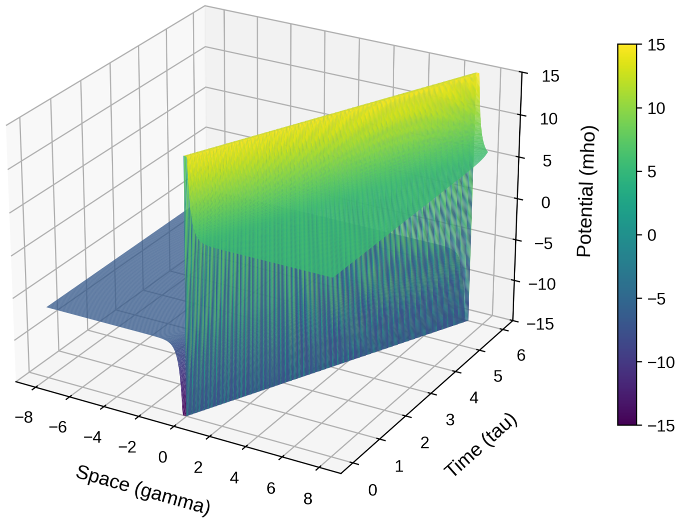

Figure 2. Coth set A

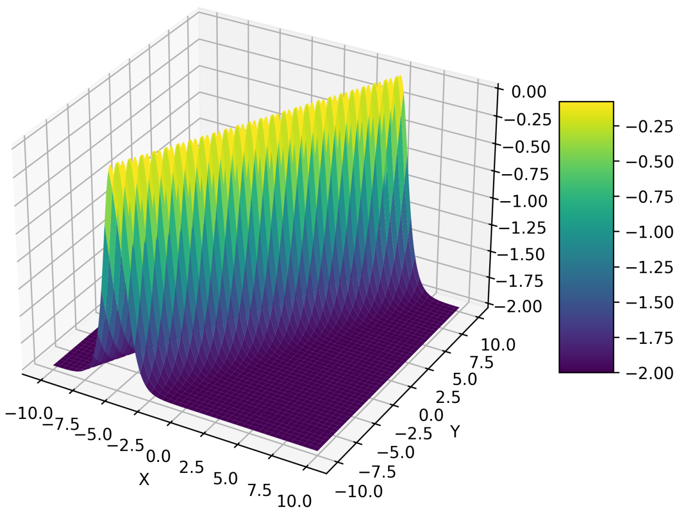

Figure 3. Tanh set B soliton profile

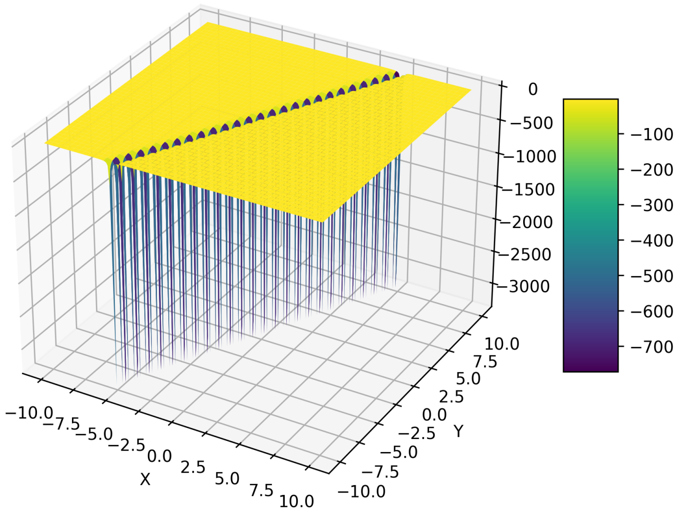

Figure 4. Coth set B soliton profile

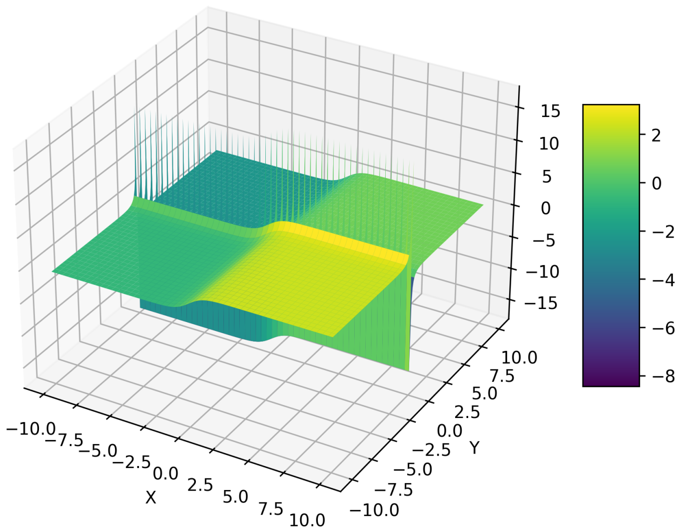

Figure 5. Mixed tanh wave structure

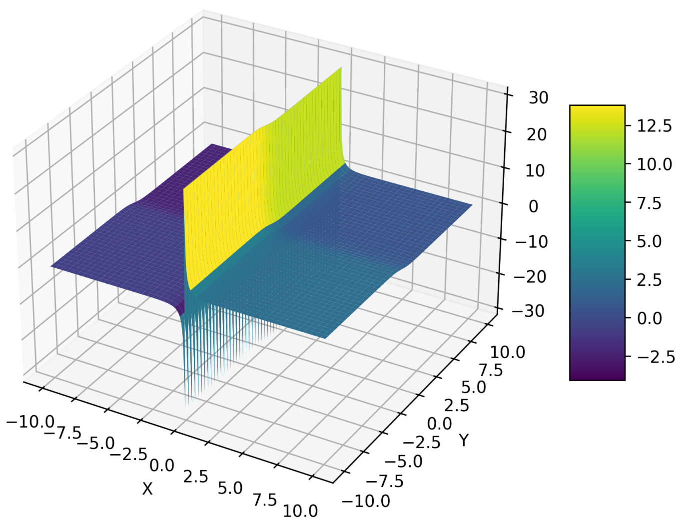

Figure 6. Mixed coth wave structure

- **Analysis of Periodic Solutions (Figures 7– 12)**

These surfaces show continuous fluctuations or “wave trains” in the plasma potential when $t < 0$. The oscillatory form of the potential is based on trigonometric functions. The recurring corrugated surface in Figures 7 and 9 (tan) indicates frequent periodic instability. Figures 8 and 10 (cot) show sharp periodic spikes that correspond to fast voltage fluctuations in the rocket nozzle. Figures 11 and 12 (mixed) show modulated oscillations in which wave interference causes the amplitude of the oscillations to change throughout the plasma field.

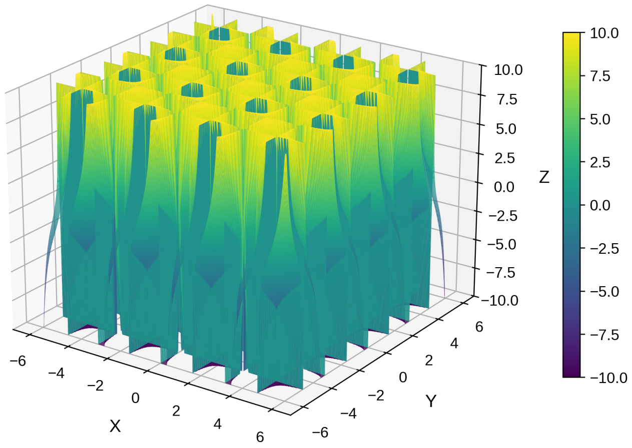

Figure 7. Tan set A

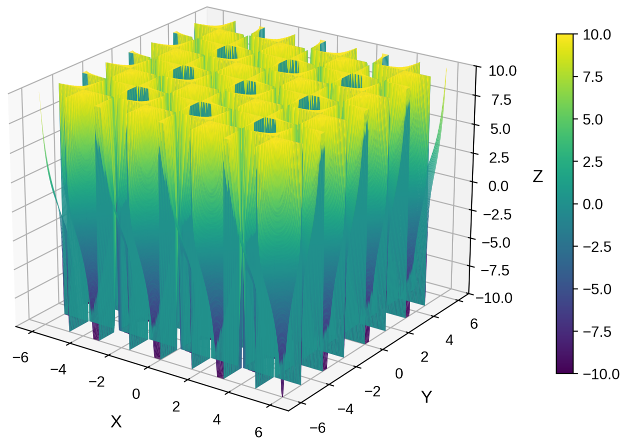

Figure 8. Cot set A

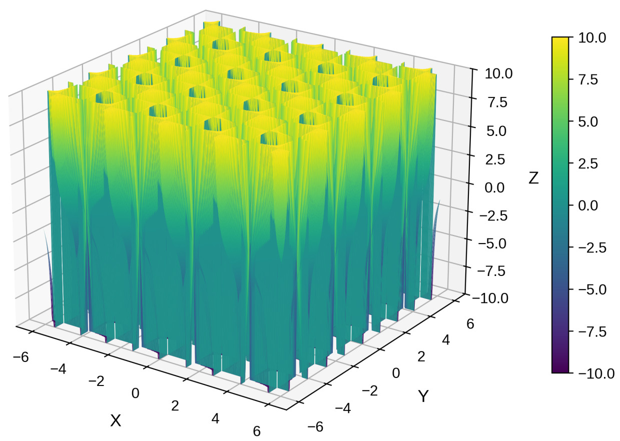

Figure 9. Tan set B

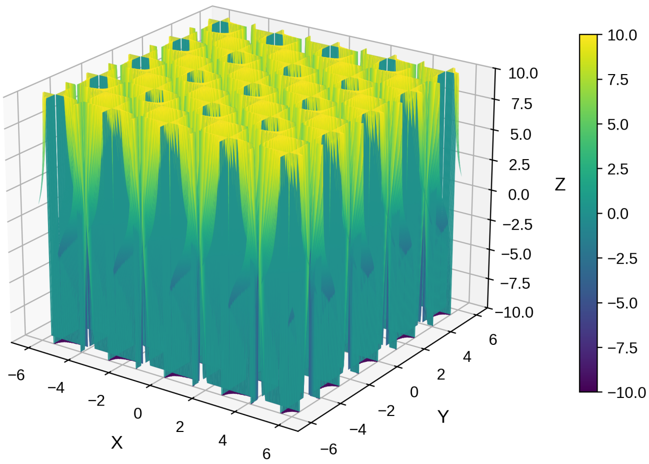

Figure 10. Cot set B

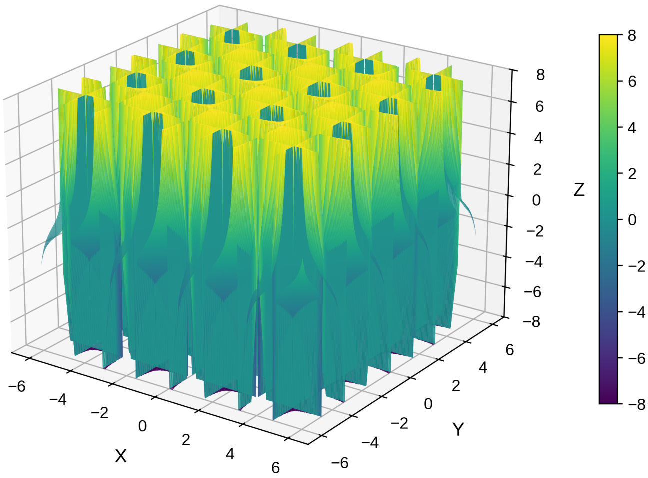

Figure 11. Mixed tan

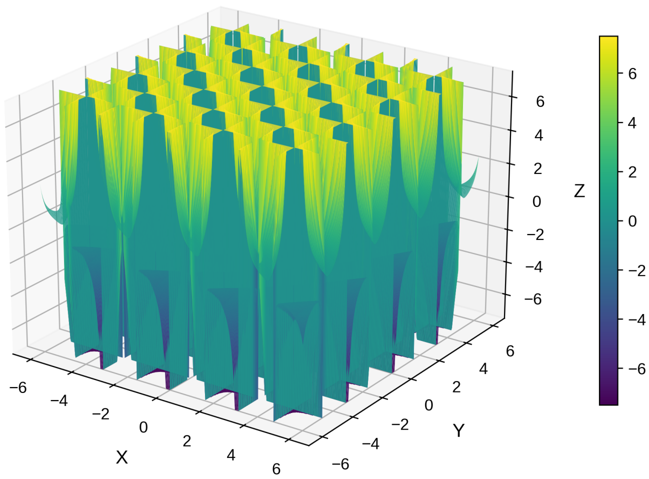

Figure 12. Mixed cot

- **Analysis of Rational and Growth Solutions (Figures 13– 15)**

These take place by direct linear transformation or at the crucial border where $t = 0$. These solutions show transition states in which waves do not form stable solitons or oscillate. Figures 13 and 14 (rational) show a single, localized "lump" that decays algebraically, signifying a transient potential disturbance that fades into the surrounding plasma. Figure 15 (linear growth) shows a non-oscillatory potential ramp and is frequently linked to a steady-state shift in the background ionization of the plume.

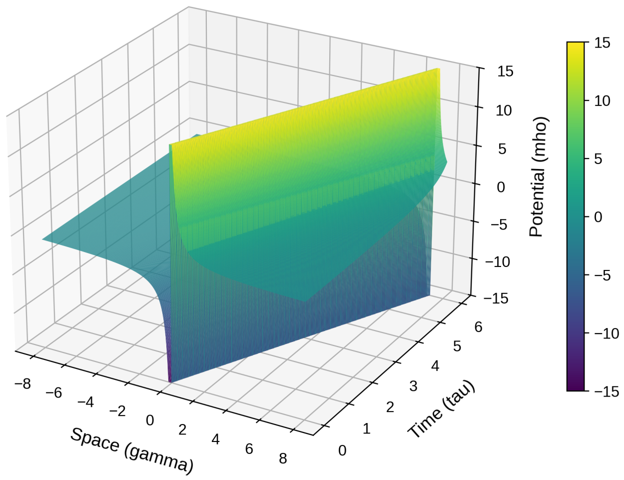

Figure 13. Rational set A

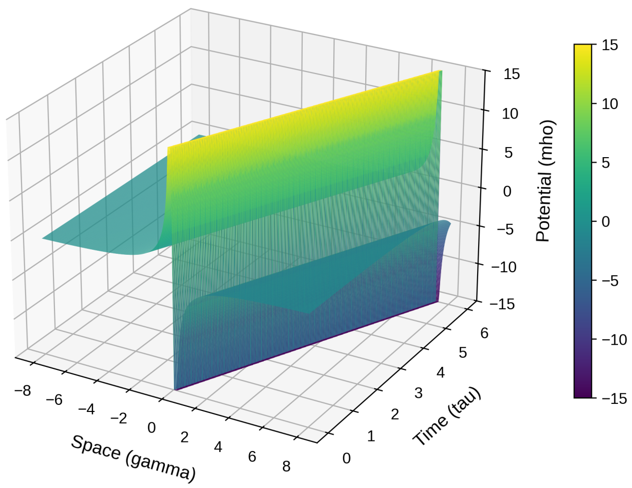

Figure 14. Rational set B

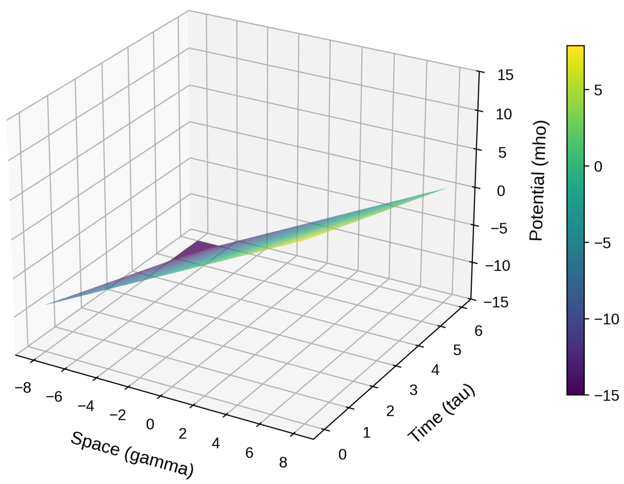

Figure 15. Linear growth

4.2 Physical Interpretations

Computational research leads to 15 different topological solutions to the modified Zakharov–Kuznetsov problem. Depending on the type of electrostatic potential α, these solutions are divided into three physical regimes. The proposed approach is innovative because it uses a generalized auxiliary ansatz equation based on a comprehensive discriminant $t = \left(\frac{\mathcal{L}^2-4\partial}{4}\right)$ in conjunction with a unified multi-dimensional wave transformation. This blended composition offers a number of special benefits.

- Simultaneous triple-regime capture: The proposed framework simultaneously extracts 15 different analytical solutions covering three completely different physical topologies (hyperbolic solitons, periodic trigonometric wave trains, and rational algebraic lumps) from a single algebraic system, rather than performing separate calculations for different wave states.
- Asymmetric and mixed structural modes: Unlike standard setups, the solver in this study introduces "Set C" mixed coefficient parameters, yielding complex hybrid models (such as Solutions C_{11} and C_{12}) that characterize multi-peaked wave structures arising from intense local plasma-wall boundaries.
- Direct mapping to plasma confinement: The transformation in this study quickly applies the analytical results to plasma diagnostic interpretations by directly connecting the mathematical coordinates to the geometry of a converging-diverging rocket nozzle.

4.2.1 Solitary wave structures ($t > 0$): Stable energy transport

Solitary waves are supported by the plasma in the regime where the discriminant t is positive. These physically correspond to localized electrostatic energy packets that move through the exhaust plume without changing form.

- Bright solitons: These appear as high-potential peaks in Solutions 1, 3, and 5. These correspond to areas of localized electron compression in a rocket nozzle, which may be a sign of significant heat strain on the nozzle walls.
- Dark solitons: These are "holes" or localized potential dips (Solutions 2, 4). When the plasma density briefly falls below the equilibrium condition, they are indicative of rarefactive ion waves.
- Singular solitons (Solutions 6, 7): The "cusp-like" peaks seen in this study are suggestive of wave-breaking occurrences, in which the dispersion is dominated by nonlinearity, frequently resulting in localized turbulence.

4.2.2 Periodic and oscillatory regimes ($t < 0$): Plasma instabilities

The solutions change into periodic trigonometric functions when t is negative. Continuous wave trains are represented by these solutions.

- Harmonic oscillations (Solutions 8–13): These solutions describe the "hum" or high-frequency instabilities that are frequently found in plasma plumes or Hall effect rockets.
- Corrugated potential surfaces: These solutions display regular, repeated ridges in their three-dimensional visualizations. These are periodic variations in the thrust vector in the context of propulsion, which, if not reduced by magnetic shielding, can cause vibration and structural fatigue.

4.2.3 Rational and transition states (t = 0)

The boundary between solitary and periodic behavior is represented by the rational answers (Answers 14 and 15). These are usually "lump" solutions, which are transient, localized disruptions. These could simulate "sparking" or brief arcs in the rocket engine brought on by abrupt changes in the ion Larmor radius or variations in the surrounding magnetic field.

4.3 Parametric Influence on Wave Morphology

For engine optimization, the electrostatic potential's sensitivity to the governing coefficients (A, B, C, and D) is crucial:

- Dispersion modulation (C, D): The solitons broaden as the Debye length grows due to the stronger dispersive effects. This suggests that the electrostatic potential is more "spread out" with lower plasma densities, lowering the possibility of localized wall erosion.
- Nonlinear effects (A, B): Narrower, higher-amplitude "bright" solitons are produced when the nonlinearity is increased by higher electron temperatures (T_e). This implies that high-intensity electrostatic spikes are more likely to occur in hotter plumes.

The physical insights drawn from the wave topologies in this study are summarized as follows:

- Plume confinement and erosion mitigation: High-intensity localized potential spike locations are captured by the bright solitary solitons (Solutions 6 and 7). These spikes show areas of high electron compression in an operational nozzle, which can accelerate plasma-wall erosion and produce localized heat hotspots. These mathematical profiles can be used by engineers to map and forecast wall damage.

- Magnetic field regulation: The proposed parametric model shows that the discriminant t, which is highly dependent on coefficient D (the ion Larmor radius effect), determines the key structural transition boundary. The findings offer a direct theoretical method for magnetic nozzle management because the Larmor radius is inversely proportional to the external magnetic field strength (B_0). Operators can drive the system into stable, predictable solitary energy packets ($t > 0$) and out of chaotic, high-frequency periodic instability regimes ($t < 0$) by actively manipulating magnetic field coils.
- Aviation communication protection: High-frequency plasma oscillations are modeled by the periodic corrugated surfaces seen when $t < 0$. During engine firings, these variations cause significant electromagnetic interference, which results in communication blackout windows. Engineers can create focused magnetic shielding techniques by using the proposed analytical framework to pinpoint the precise thrust and density thresholds that cause these instabilities.

5 Conclusions

The nonlinear dynamics of electrostatic potential waves within rocket engine plasma plumes, modeled by the modified Zakharov–Kuznetsov equation, were effectively investigated in this study using a reliable computer solver. This study obtained fifteen precise analytical solutions describing the intricate behavior of ionized gases in magnetized nozzle environments by combining an advanced wave transformation with an ansatz-based methodology. For solitary wave solutions ($t > 0$), the study divided these solutions into three different physical regimes. Understanding localized heat flow on nozzle surfaces requires the demonstration of stable, localized energy packets (bright, dark, and solitary solitons) that can move through the exhaust without dissipating. For periodic oscillations ($t < 0$), wave trains and high-frequency instabilities that indicate periodic potential fluctuations were found; these are crucial for identifying electromagnetic interference in communication systems. For rational solutions ($t = 0$), the transition between stable and unstable plasma states is represented by captured transient disturbances. The parametric analysis showed that the Debye length and the ion Larmor radius had a significant impact on the morphology of these waves, particularly their amplitude and width. These results imply that engineers can successfully regulate the change from chaotic instabilities to stable energy transport by varying the external magnetic field of a plasma thruster. In the end, this computational framework offers a theoretical standard for designing and refining next-generation propulsion systems based on plasma. In order to improve the forecast accuracy in a variety of aerospace situations, future work will concentrate on expanding this model to incorporate collisional effects and non-thermal ion distributions.

The highlights of this study are as follows:

- Advanced modeling: Successfully modeled three-dimensional electrostatic potential waves in magnetized rocket plasma using the modified Zakharov–Kuznetsov equation.
- Novel computational approach: Implemented a unified wave transformation and ansatz-based solver to derive 15 distinct exact analytical solutions.
- Diverse wave topologies: Characterized stable bright/dark solitons, periodic wave trains, and rational “lump” solutions within the exhaust plume.
- Parametric sensitivity: Quantified the influence of ion Larmor radius and Debye length on wave stability and energy localization.
- Propulsion application: Provided a theoretical framework for mitigating plasma instabilities and optimizing magnetic nozzle efficiency in aerospace systems.

Data Availability

The data used to support the research findings are available from the corresponding author upon request.

Conflicts of Interest

The author declares no conflicts of interest.

References

[1] H. Gong, H. Fang, and Z. Li, “Numerical simulation of ionospheric disturbances due to rocket plume and its influence on HF radio waves propagation,” *Universe*, vol. 8, no. 6, p. 331, 2022. https://doi.org/10.3390/universe8060331

[2] S. Islam, M. N. Alam, M. F. Al-Asad, and C. Tunc, “An analytical technique for solving new computational solutions of the modified Zakharov–Kuznetsov equation arising in electrical engineering,” *J. Appl. Comput. Mech.*, vol. 7, no. 2, pp. 715–726, 2021. https://doi.org/10.22055/jacm.2020.35571.2687

[3] G. Cai, L. Liu, B. He, G. Ling, H. Weng, and W. Wang, “A review of research on the vacuum plume,” *Aerospace*, vol. 9, no. 11, p. 706, 2022. https://doi.org/10.3390/aerospace9110706

[4] J. L. Suazo Betancourt, N. Butler-Craig, J. Lopez-Uricoechea, J. Bak, D. Lee, A. M. Steinberg, and M. L. R. Walker, "Thomson scattering measurements in the krypton plume of a lanthanum hexaboride hollow cathode in a large vacuum test facility," *J. Appl. Phys.*, vol. 135, no. 8, p. 083302, 2024. https://doi.org/10.1063/5.0180251

[5] W. van Lynden, R. Andriulli, N. Souhair, F. Ponti, and M. Magarotto, "Coupling of fluid and particle-in-cell simulations of ambipolar plasma thrusters," *Aerospace*, vol. 11, no. 11, p. 880, 2024. https://doi.org/10.3390/aerospace11110880

[6] K. Arif, T. Ehsan, W. Masood, S. Asghar, H. A. Alyousef, E. Tag-Eldin, and S. A. El-Tantawy, "Quantitative and qualitative analyses of the mKdV equation and modeling nonlinear waves in plasma," *Front. Phys.*, vol. 11, p. 1118786, 2023. https://doi.org/10.3389/fphy.2023.1118786

[7] H. Mushtaq, K. Singh, S. Zaheer, and I. Kourakis, "Nonlinear ion-acoustic waves with Landau damping in non-Maxwellian space plasmas," *Sci. Rep.*, vol. 14, p. 13005, 2024. https://doi.org/10.1038/s41598-024-63773-7

[8] A. A. Zaagan, A. Altalbe, and A. Bekir, "Dynamical analysis and soliton solutions of a variety of quantum nonlinear Zakharov–Kuznetsov models via three analytical techniques," *Front. Phys.*, vol. 12, p. 1427827, 2024. https://doi.org/10.3389/fphy.2024.1427827

[9] A. Palit, A. Roy, and S. Raut, "Qualitative studies of the influence of damping and external periodic force on ion-acoustic waves in a magnetized dusty plasma through modified ZK equation," *Braz. J. Phys.*, vol. 52, p. 110, 2022. https://doi.org/10.1007/s13538-022-01083-x

[10] K. K. Ali, A. R. Seadawy, A. Yokus, R. Yilmazer, and H. Bulut, "Propagation of dispersive wave solutions for (3 + 1)-dimensional nonlinear modified Zakharov–Kuznetsov equation in plasma physics," *Int. J. Mod. Phys. B*, vol. 34, no. 25, p. 2050227, 2020. https://doi.org/10.1142/s0217979220502276

[11] W. Alhejaili, S. Roy, S. Raut, A. Roy, A. H. Salas, T. Aboelenen, and S. A. El-Tantawy, "Analytical solutions to (modified) Korteweg–de Vries–Zakharov–Kuznetsov equation and modeling ion-acoustic solitary, periodic, and breather waves in auroral magnetoplasmas," *Phys. Plasmas*, vol. 31, no. 8, p. 082107, 2024. https://doi.org/10.1063/5.0220798

[12] M. Junaid-U-Rehman, H. Almusawa, J. Awrejcewicz, G. Kudra, N. Abbas, and A. Rasool, "Propagation of electrostatic potential with dynamical behaviors and conservation laws of the (3+1)-dimensional nonlinear extended quantum Zakharov–Kuznetsov equation," *Int. J. Geom. Methods Mod. Phys.*, vol. 21, no. 01, p. 2450032, 2024. https://doi.org/10.1142/s0219887824500324

[13] M. Al-Amin, M. N. Islam, O. A. İlhan, M. A. Akbar, and D. Soybaş, "Solitary wave solutions to the modified Zakharov–Kuznetsov and the (2+1)-dimensional Calogero–Bogoyavlenskii–Schiff models in mathematical physics," *J. Math.*, vol. 2022, no. 1, p. 5224289, 2022. https://doi.org/10.1155/2022/5224289

[14] M. Areshi, A. R. Seadawy, A. Ali, A. F. AlJohani, W. Alharbi, and A. F. Alharbi, "Construction of solitary wave solutions to the (3 + 1)-dimensional nonlinear extended and modified quantum Zakharov–Kuznetsov equations arising in quantum plasma physics," *Symmetry*, vol. 15, no. 1, p. 248, 2023. https://doi.org/10.3390/sym15010248

[15] A. H. Ganie, F. Mofarreh, and A. Khan, "A fractional analysis of Zakharov–Kuznetsov equations with the Liouville–Caputo operator," *Axioms*, vol. 12, no. 6, p. 609, 2023. https://doi.org/10.3390/axioms12060609

[16] H. R. Nabi, H. F. Ismael, N. A. Shah, and W. Weera, "W-shaped soliton solutions to the modified Zakharov–Kuznetsov equation of ion-acoustic waves in (3+1)-dimensions arise in a magnetized plasma," *AIMS Math.*, vol. 8, no. 2, pp. 4467–4486, 2023. https://doi.org/10.3934/math.2023222

[17] F. U. Afrin, "Solitary wave solutions and investigation the effects of different wave velocities of the nonlinear modified Zakharov–Kuznetsov model for the wave propagation in nonlinear media," *Partial Differ. Equ. Appl. Math.*, vol. 8, p. 100583, 2023. https://doi.org/10.1016/j.padiff.2023.100583

[18] D. Lu, M. Suleman, J. Ul Rahman, S. Noeiaghdam, and G. Murtaza, "Numerical simulation of fractional Zakharov–Kuznetsov equation for description of temporal discontinuity using projected differential transform method," *Complexity*, vol. 2021, no. 1, p. 9998610, 2021. https://doi.org/10.1155/2021/9998610

[19] E. H. M. Zahran, R. A. Ibrahim, D. U. Ozsahin, H. Ahmad, and M. S. M. Shehata, "New diverse exact optical solutions of the three dimensional Zakharov–Kuznetsov equation," *Opt. Quantum Electron.*, vol. 55, p. 817, 2023. https://doi.org/10.1007/s11082-023-04909-3

[20] M. Alqhtani, K. M. Saad, R. Shah, and W. M. Hamanah, "Discovering novel soliton solutions for (3+1)-modified fractional Zakharov–Kuznetsov equation in electrical engineering through an analytical approach," *Opt. Quantum Electron.*, vol. 55, p. 1149, 2023. https://doi.org/10.1007/s11082-023-05407-2